Stereoelectronic Effects on Molecular Geometries and State-Energy Splittings of Ligated Monocopper Dioxygen Complexes

Christopher J. Cramer,*,† Jeffrey R. Gour,‡ Armagan Kinal,§ Marta Włoch,‡,|| Piotr Piecuch,‡,⊥ Abdul Rehaman Moughal Shahi,# and Laura Gagliardi#

Department of Chemistry and Supercomputer Institute, University of Minnesota, 207 Pleasant Street SE, Minneapolis, Minnesota 55455, Department of Chemistry and Department of Physics and Astronomy, Michigan State University, East Lansing, Michigan 48824, Department of Chemistry, Ege University, 35100 Bornova/Izmir, Turkey, and Department of Physical Chemistry, Sciences II University of Geneva, 30 Quai Ernest Ansermet, CH-1211 Geneva 4, Switzerland

Received: January 22, 2008

The relative energies of side-on versus end-on binding of molecular oxygen to a supported Cu(I) species, and the singlet versus triplet nature of the ground electronic state, are sensitive to the nature of the supporting ligands and, in particular, depend upon their geometric arrangement relative to the O_2 binding site. Highly correlated ab initio and density functional theory electronic structure calculations demonstrate that optimal overlap (and oxidative charge transfer) occurs for the side-on geometry, and this is promoted by ligands that raise the energy, thereby enhancing resonance, of the filled Cu d_{xz} orbital that hybridizes with the in-plane π^* orbital of O_2. Conversely, ligands that raise the energy of the filled Cu d_{z^2} orbital foster a preference for end-on binding as this is the only mode that permits good overlap with the in-plane O_2 π^*. Because the overlap of Cu d_{z^2} with O_2 π^* is reduced as compared to the overlap of Cu d_{xz} with the same O_2 orbital, the resonance is also reduced, leading to generally more stable triplet states relative to singlets in the end-on geometry as compared to the side-on geometry, where singlet ground states become more easily accessible once ligands are stronger donors. Biradical Cu(II)-O_2 superoxide character in the electronic structure of the supported complexes leads to significant challenges for accurate quantum chemical calculations that are best addressed by exploiting the spin-purified M06L local density functional, single-reference completely renormalized coupled-cluster theory, or multireference second-order perturbation theory, all of which provide predictions that are qualitatively and quantitatively consistent with one another.

Introduction

The activation of molecular oxygen by coordination to supported Cu(I) ions is a ubiquitous theme in both biological and inorganic catalysis,[1−8] owing in part to useful ranges of redox properties and coordination motifs that are associated with the intermediate CuO_2 species.[9−35] From a redox perspective, the coordination of molecular oxygen to a supported LCu(I) species (where we use L generically to represent a single ligand or multiple ligands) may be considered formally to proceed either without a change of the copper oxidation state or with one or two electrons transferred from the metal resulting in formal LCu(II)O_2(−) and LCu(III)O_2(2−) products, respectively. As molecular oxygen itself has a triplet electronic ground state, one might expect relatively weakly coupled LCu(I)O_2 species also to have triplet ground states, and the singlet and triplet states might be expected to have similar energies for the biradical-like LCu(II)O_2(−) species, depending on the nature of the coupling between the open-shell d^9 Cu(II) ion and the superoxide radical anion. The LCu(III)O_2(2−) species, on the other hand, would be expected to have singlet ground states given the closed-shell character of typical d^8 copper complexes and the peroxide dianion.

Of course, the nature of the coupling between the two fragments, LCu and O_2, depends on the nature of the ligand(s) L, and the coordination geometry of the O_2 fragment, either end-on or side-on. Moreover, covalent character in the Cu−O bonding can lead to electronic structures best viewed as intermediate between pairs of formal oxidation states.[8,11,16,35] Scheme 1 illustrates those cases for which significant structural and spectral data are available. The first case, **1**, is an end-on precatalytic complex of O_2 in the Cu_B site of peptidylglycine α-hydroxylating monooxygenase (PHM). A single-crystal X-ray structure[19] having 1.8 Å resolution is available for this case of Cu supported by two histidine residues and one methionine. The O−O bond length is reported to be 1.23 Å, which is only very slightly longer than that of molecular oxygen (1.207 Å),[36] suggesting that the correct formulation for this species would be likely to be Cu(I)O_2 (i.e., there is little charge transfer from the metal to the O_2 fragment). Compound **2** also has been established by X-ray crystallography to bind O_2 end-on,[32] and its ground electronic state has been confirmed to be a triplet.[35] Structure **2** was originally assigned, incorrectly, to have a singlet ground state,[20] based in part on density functional calculations, which nicely illustrates the significant challenges that $LCuO_2$ systems can pose for computation. In the case of compound **3**, no crystal structure has been obtained, but resonance Raman

* Corresponding author. E-mail: cramer@umn.edu.
† University of Minnesota.
‡ Department of Chemistry, Michigan State University.
§ Ege University.
|| Present address: Department of Chemistry, Michigan Technological University, 1400 Townsend Dr., Houghton, MI 49931.
⊥ Department of Physics and Astronomy, Michigan State University.
University of Geneva.

10.1021/jp800627e CCC: $40.75 © 2008 American Chemical Society
Published on Web 03/15/2008

SCHEME 1

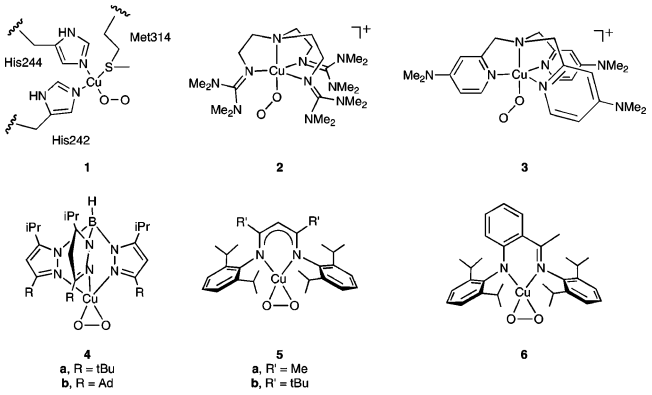

data support an end-on binding mode; the electronic ground state has not been determined.[34]

In contrast to the end-on species **1**−**3**, compounds **4a** and **4b** have been determined to have their O_2 fragments bound in a side-on fashion. Their electronic structures have been assigned to be singlet ground states having a dominant $LCu(II)O_2(-)$ character based on the O−O bond length in **4a** from X-ray crystallography,[9,11] the O−O stretching frequency (which has been shown[8,11] to be well correlated by Badger's rule[37] with the O−O bond length) from resonance Raman spectra for **4a** and **4b**,[9,12,31] and K- and L_3-edge X-ray absorption spectroscopy (XAS) for **4b**.[12,31] Compounds **5b**[10] and **6**[23] also have been determined by X-ray crystallography to bind O_2 side-on, but the singlet ground states for these species have been assigned to be dominated by $LCu(III)O_2(2-)$ character based on O−O bond lengths, stretching frequencies (available also for **5a**[38] and essentially identical to that for **5b**), and K- and L_3-edge XAS for **5a**.[31]

Thus, over an array of different ligands, it is evidently possible to access the full range of Cu(I), Cu(II), or Cu(III) oxidation states, both O_2 coordination motifs, and either singlet or triplet ground states. An interesting question is the degree to which these different phenomena will affect the reactivity of the different complexes, especially with respect to the activation of C−H bonds. Theoretical models might be expected to play a useful role in assessing this situation. However, as noted above, the application of routine modeling protocols (e.g., density functional theory (DFT)) is not necessarily straightforward and can lead to erroneous predictions.

The key challenge in the modeling of $LCuO_2$ systems is that they can exhibit substantial multideterminantal character, particularly when the biradicaloid $LCu(II)O_2(-)$ mesomer contributes significantly to the valence-bond description of the electronic structure.[10,14,16,20,22,23,25−30,39] This multideterminantal character makes the application of Kohn−Sham (KS) density functional theory problematic since a single determinant is fundamental to the model.[40] This tends to lead to the destabilization of singlet states relative to triplet states (as the high-spin versions of the latter are usually well represented by single determinants) and also introduces significant sensitivity to the amount of exact Hartree−Fock (HF) exchange that may or may not be included in a particular functional.[40,41]

This problem is precisely analogous to that which can arise in dimeric, as opposed to monomeric, $(LCu)_2O_2$ complexes. In that case, there is substantial biradical character in a $[LCu(II)]_2O_2(2-)$ formulation, and predicting the energies of such structures relative to others where more closed-shell wave functions dominate (e.g., $[LCu(III)]_2O(2-)_2$) can be especially challenging.[42−53] Multiconfigurational models (e.g., employing

SCHEME 2

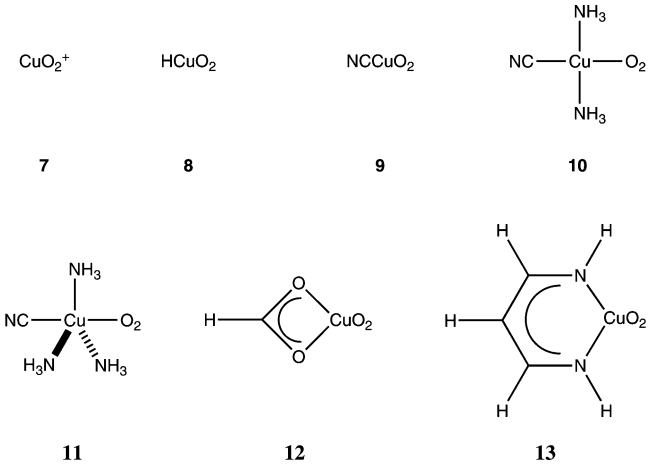

complete active-space self-consistent field (CASSCF) wave functions or subsequent multiconfigurational second-order perturbation theory (CASPT2)) are not necessarily practical in this instance given the very large numbers of electrons and orbitals that may be necessary to construct a balanced active space. Nevertheless, in previous studies of $(LCu)_2O_2$ cases, we found that careful comparisons of multiconfigurational calculations with DFT and completely renormalized coupled-cluster (CR-CC) calculations were particularly useful for elucidating key electronic structural details and moreover for validating specific density functional protocols.[50,51] For monomeric $LCuO_2$, we expect this approach to be equally informative and indeed perhaps more so since multiconfigurational approaches now need to contend with the valence space of only a single copper atom.

Thus, in this article, we report comparisons of predictions from CR-CC, CASPT2, and DFT calculations for the prediction of O_2 binding modes and state energies for a series of $LCuO_2$ model complexes. In particular, we examine the species **7**−**13** listed in Scheme 2. On the basis of our results, we identify ligand features that play decisive roles in determining the coordination motif and electronic ground state.

Computational Methods

Basis Sets. Two different basis sets including a copper relativistic core pseudopotential (the Stuttgart 10-electron pseudopotential and associated basis functions ECP10MWB[54]) were used in this work, and we will refer to these as BS1 and BS2. The smaller BS1 basis set was used only for the generation of molecular geometries and employed the Stuttgart [8s7p6d|6s5p3d] contraction for Cu and the 6-31G(d) basis set for H, N, C, and O. In the single case of $HCuO_2$ geometries, the 6-31G(d,p) basis set[55] was used in place of 6-31G(d) for H and O. The larger BS2 basis set was used for all single-point energy calculations on optimized geometries. The BS2 basis set employed the Stuttgart [8s7p6d2f|6s5p3d2f] contraction for Cu and the atomic natural orbital (ANO) basis set of Widmark et al.[56] contracted [14s9p4d|4s3p2d] for C, N, and O and [8s4p|2s1p] for H.

Density Functionals. We examined three different local density functionals in this work and four hybrid functionals. The BLYP functional combines the generalized-gradient approximation (GGA) exchange functional of Becke[57] with the GGA correlation functional of Lee et al.[58] The *m*PW functional combines the GGA exchange[59] and correlation[60] functionals of Perdew and Wang as modified by Adamo and Barone.[61] The

M06L functional is a meta-GGA functional.[62] The hybrid HF-DFT functionals[63] that we considered included B3LYP,[64] *m*PW1,[61] M06,[65] and M06-2X,[65] which incorporate 20, 25, 27, and 54% HF exchange, respectively, into their corresponding functionals.

For singlet-state calculations, lowest-energy restricted (R) self-consistent field (SCF) solutions were obtained and then checked for instability. Unstable RSCF solutions were reoptimized at the unrestricted (U) SCF level.[40] Spin purification[66,67] was employed to eliminate triplet-state spin contamination from these broken-spin symmetry (BS) SCF solutions. In this approach, the singlet energy is computed as[68−71]

$$E_{\text{singlet}} = \frac{2E_{\langle S_z\rangle=0} - \langle S^2\rangle E_{\langle S_z\rangle=1}}{2 - \langle S^2\rangle} \quad (1)$$

where the triplet energy is computed for the single-determinantal high-spin configuration $S_z = 1$ (at the UDFT level), and $\langle S^2\rangle$ is the expectation value of the total-spin operator applied to the KS determinant for the unrestricted $S_z = 0$ calculation. Gräfenstein and Cremer[72] have shown that values of $\langle S^2\rangle$ computed at the DFT level have diagnostic value in assessing spin contamination so that the spin-purified (sp) approach is more physically realistic than using the raw BS energy.

Single-Reference Post-SCF Levels. We performed single-reference CC calculations[73,74] using the standard CC method with singles and doubles (CCSD)[75−77] and, to obtain a quantitative description, the rigorously size extensive variant of the completely renormalized (CR) CC theory[78−88] with singles, doubles, and non-iterative triples, termed CR-CC(2,3),[85−88] in which one adds a robust a posteriori correction due to triply excited clusters to the CCSD energy. Prior work on molecules containing $Cu_2O_2^{2+}$ cores has demonstrated that the CR-CC(2,3) level can predict accurate relative energies for isomers differing significantly in their degree of biradical character.[50,51] Several other benchmark studies and applications have shown that in spite of its single-reference character, the CR-CC(2,3) approach is capable of providing a highly accurate description of the lowest-energy singlet and triplet states of biradicals and systems undergoing significant bond rearrangements,[84−92] where the conventional CC methods, such as CCSD and CCSD(T),[93] fail or have considerable problems. On the basis of this positive experience, we regard the CR-CC(2,3) level as a reference level for assessing the accuracy of other methods used in the present study.

In all single-reference correlated calculations, we used as a reference the RHF (singlet) or ROHF (triplet) determinant that we identified as the lowest-energy symmetry-adapted SCF solution. In all CC calculations, we explicitly correlated the 4s and 3d electrons of the Cu atoms, the 2s and 2p electrons of the C, N, and O atoms, and the 1s electrons of the H atoms.

Multiconfigurational SCF and Post-SCF Levels. The complete active space (CAS) SCF method[94] was used to generate molecular orbitals (MOs) and reference functions for subsequent multiconfigurational second-order perturbation calculations of the dynamic correlation energy (CASPT2).[95] In CASPT2 calculations, C, N, and O 1s orbitals and Cu orbitals up to 3s were kept frozen. In addition, all such calculations employed a real level shift[96] of 0.1 au in combination with a technique[97] that shifts active space orbital energies to simulate ionization energies for orbitals from which excitations are taking place and electron affinities for orbitals into which excitations are taking place.

Calculations were performed using two active spaces, either 18 electrons in 16 orbitals or 16 electrons in 15 orbitals. The orbitals of the 18/16 active space are linear combinations of Cu 3d and 4d atomic orbitals (AOs; 10) with O 2p AOs (6). The importance of including a double shell of d orbitals on late transition metals such as Cu to adequately correlate the d space has been noted previously.[98,99] The 16/15 active space is obtained from the 18/16 space by eliminating the lowest doubly occupied orbital, which is mainly O 2p in character and appears to introduce some instability in those cases supported by the largest number or most strongly electron-donating ligands.

TABLE 1: Cu−O and O−O Bond Lengths (Å) for End-On and Side-On Geometries of 7−13[a]

	end-on		side-on	
structure	*r*Cu−O	*r*O−O	*r*Cu−O	*r*O−O
7	1.909	1.240	2.056	1.275
8	1.880	1.264	2.035	1.291
9	1.845	1.263	1.990	1.300
10	1.964	1.309	2.088	1.289
11	1.964	1.315	2.555	1.265
12	1.822	1.280	1.914	1.341
13	1.854	1.285	1.890	1.366

[a] Geometries from BS U*m*PW91/BS1 optimizations; see Computational Methods section.

Geometries. For each set of ligands, end-on and side-on bound CuO_2 complexes were optimized for singlet electronic states at the broken-symmetry U*m*PW91/BS1 level. Optimized structures for $\mathbf{7}_{\text{side}}$, $\mathbf{8}_{\text{side}}$, $\mathbf{9}_{\text{side}}$, $\mathbf{10}_{\text{side}}$, $\mathbf{12}_{\text{side}}$, and $\mathbf{13}_{\text{side}}$ belong to the C_{2v} point group; all other optimized structures belong to the C_s point group. In the cases of $\mathbf{10}_{\text{end}}$, $\mathbf{10}_{\text{side}}$, $\mathbf{12}_{\text{end}}$, and $\mathbf{13}_{\text{end}}$, the O_2 fragments lie in symmetry planes that are themselves perpendicular to the planes containing the remaining heavy atoms; attempts to optimize alternative BS singlet end-on structures with O_2 fragments in the planes of the remaining heavy atoms led in each case only to the higher symmetry side-on geometries. Cartesian coordinates for all optimized structures are provided as Supporting Information. As our goal in this paper is to examine singlet−triplet energy differences as a function of theoretical protocol, and not to predict accurate adiabatic singlet−triplet splittings for the hypothetical molecules **7**−**13**, the singlet geometries were used for all calculations.

Software. Full details on software are provided in the Supporting Information.

Results

CuO_2^+. We begin by considering the unsupported cationic complex between Cu(I) and molecular oxygen. In the end-on geometry, the Cu−O bond is 1.909 Å, and the O−O bond is 1.240 Å. In the side-on geometry, the Cu−O bonds are 2.056 Å and the O−O bond is 1.275 Å. For convenience, these bond lengths are tabulated for all geometries of **7**−**13** in Table 1. The energies of the singlet and triplet states for both geometries relative to the end-on triplet, and the absolute energy of the end-on triplet, are listed in Table 2 for various levels of theory.

Geometrically speaking, the optimized singlet geometries suggest only weak charge transfer from the Cu(I) to the O_2 fragment since the predicted O−O bond lengths are only slightly extended from the equilibrium value for $^1\Delta$ O_2, 1.216 Å.[36] Similarly, the predicted singlet−triplet (S−T) splittings for the two geometries (24.1 and 27.0 kcal mol^{-1} at the reference CR-CC(2,3) level for the end-on and side-on structures, respectively) are similar to the adiabatic value for O_2 itself, 22.5 kcal mol^{-1}. Thus, a Cu(I)O_2 formulation seems to be the best description of the bare system.

With respect to the isomer energetics, all of the correlated levels of theory make similar predictions for the relative energies

TABLE 2: Absolute (E_h) and Relative (kcal mol^{-1}) Electronic Energies for Singlet and Triplet 7_{end} and 7_{side}[a]

	7_{end}		7_{side}	
level of theory	triplet (E_{abs})	singlet (E_{rel})	triplet (E_{rel})	singlet (E_{rel})
R(O)HF	−345.581 88	39.1	16.7	53.5
CCSD	−346.324 71	26.3	7.9	36.1
CR-CC(2,3)	−346.358 55	24.1	6.1	33.1
CAS(18,16)	−345.842 12	14.1	9.0	23.8
CASPT2(18,16)	−346.333 13	27.7	7.2	36.6
RBLYP[b]		21.9		39.5
UBLYP	−347.385 36	7.1	6.2	14.5
spBLYP		13.9		22.9
R*m*PW		23.2		39.9
U*m*PW	−347.514 53	7.2	5.7	14.0
sp*m*PW		14.1		22.2
RM06L		27.4		42.4
UM06L	−347.424 92	12.2	4.6	18.1
spM06L		23.9		31.7
RB3LYP		29.5		43.1
UB3LYP	−347.427 33	9.4	6.7	16.9
spB3LYP		18.7		27.3
R*m*PW1		32.5		45.2
U*m*PW1	−347.393 28	9.8	6.6	17.1
sp*m*PW1		19.5		27.8
RM06		28.7		43.4
UM06	−347.374 30	15.0	6.9	23.0
spM06		29.7		39.2
RM06-2X		32.0		42.6
UM06-2X	−347.405 49	14.1	7.4	21.7
spM06-2X		28.0		36.2

[a] See Computational Methods for details on basis set, geometries, etc. Singlet $\langle S^2 \rangle$ values used for computation of spin-purified DFT singlet energies are provided in the Supporting Information. [b] DFT energies are reported for restricted (R), unrestricted (U), and spin-purified (sp) protocols, where triplet energies are only from the unrestricted formalism, while singlet energies may be R, U (implying the use of raw broken-symmetry energies), or sp (see eq 1).

of the two triplets, both of which are well described by single determinants. Curiously, M06L predicts a somewhat smaller splitting than the other DFT levels, but the DFT models span either side of the CR-CC(2,3) prediction, so it is not obvious that any one number is more correct than another. With respect to the relative singlet energies, CR-CC(2,3) and CASPT2 put the end-on and side-on singlets roughly 25 and 35 kcal mol^{-1}, respectively, above the end-on triplet. Predictions from RDFT are in modestly good agreement with these two values, generally overestimating the state energies by a few kcal mol^{-1} for the end-on singlet and by larger margins for the side-on singlet. Raw BS singlet energies significantly underestimate the state energies, consistent with the BS SCF solutions containing substantial character from the much lower energy triplet. Spin purification improves the state-energy estimates, but they remain significantly underestimated by all DFT models except those in the M06 family. It is informative to compare all of these state energies graphically, and this is done in Figure 1. From Figure 1, it is straightforward to note, for instance, that spM06L shows a markedly better performance than any other DFT functional and that CASPT2 agrees with CR-CC(2,3) well except that there is a modest systematic overestimation of singlet energies as compared to triplets, which is a well-known feature of the CASPT2 model in, say, carbenes.[100]

$HCuO_2$. The simplest of the family of anionic ligands that we examine here is the hydride anion. In this case, the end-on geometry has a Cu−O bond length of 1.880 Å and the O−O bond is 1.264 Å, while the side-on geometry has Cu−O bond lengths of 2.035 Å, and the O−O bond is 1.291 Å. The changes relative to the bare system indicate additional charge transfer to the O_2 fragment as a result of hydride ligation, but the effect remains relatively weak as judged by the still very short O−O bonds. Consistent with this assessment, the S−T splittings are reduced from those computed for **7** and molecular O_2 by only about 5 kcal mol^{-1} at the correlated levels of theory. In the interest of brevity, the raw data for **8** analogous to those in Table 1 are provided in the Supporting Information (Table S-1); Figure 2 summarizes those data in graphical form, except that raw, unrestricted broken-symmetry singlet energies are not included.

The introduction of the hydride ligand does perturb the end-on/side-on equilibrium somewhat as compared to **7**. At the CR-CC(2,3) and CASPT2 levels, the triplet-state preference for the end-on geometry is reduced to about 2 kcal mol^{-1}; the DFT models predict near degeneracy. A similar stabilization of the side-on singlet relative to the end-on geometry is also predicted, with the effect being slightly larger in magnitude.

As with **7**, the RDFT models make predictions that are in fair agreement with CR-CC(2,3) and CASPT2, although it is now more evident that local functionals (those not including HF exchange) offer an improved agreement as compared to the hybrids. Indeed, with increased HF exchange, the singlet states are systematically moved to higher and higher energies at the RB3LYP, R*m*PW1, RM06, and RM06-2X levels. Raw broken-symmetry singlet energies are again in very poor agreement with the benchmark CR-CC(2,3) and CASPT2 levels because of triplet spin contamination. In the case of **8**, however, spin purification provides less uniform results than was true for **7**. spBLYP and sp*m*PW underestimate the singlet-state energies by 6−8 kcal mol^{-1}, while the other local functional, spM06L, is in quantitatively good agreement with CR-CC(2,3) and CASPT2. The hybrid functionals show systematic overestimation of the side-on singlet energies after spin purification, while they show less uniform behavior for the end-on singlet. Interestingly, all DFT levels predict the end-on singlet to be lower in energy than the side-on singlet, while CR-CC(2,3) and CASPT2 predict that order to be reversed, albeit by only a small margin.

$NCCuO_2$. As a next step from hydride, we considered the nitrile ligand. However, as can be seen from the comparison of Figure 3 to Figure 2 (raw data may be found in Table S-2 of the Supporting Information), these two ligands have an essentially identical influence (or lack thereof) on the coordination and state-energy preferences of the CuO_2 fragment. This observation holds for all levels of theory. With respect to geometries, the geometry of $\mathbf{9}_{end}$ is very similar to that of $\mathbf{8}_{end}$ with a Cu−O bond length of 1.845 Å and an O−O bond of 1.263 Å. For the side-on geometry, the nitrile appears to be a slightly better donor than the hydride, so that $\mathbf{9}_{side}$ has Cu−O bond lengths of 1.990 Å and an O−O bond of 1.300 Å. A noteworthy feature of Figure 3 is the remarkably good performance of spM06L for the relative singlet energies, when compared to the CR-CC(2,3) reference data.

$NC(NH_3)_2CuO_2$. To assess the influence of additional ligands beyond a single anionic donor, we next added two neutral ammonia ligands to **9** to generate **10**. We enforced coplanarity of the Cu, C, and N atoms in $\mathbf{10}_{side}$ (the C_{2v} isomer with all heavy atoms in the plane was higher in energy), and it was effectively maintained for these same atoms plus the proximal O atom in $\mathbf{10}_{end}$. Thus, the coordination geometry about Cu is best described as trigonal bipyramidal in $\mathbf{10}_{side}$ (although the η^2 O_2 fragment has a O−Cu−O bond angle of only 36°) and square planar in $\mathbf{10}_{end}$. In $\mathbf{10}_{side}$, the Cu−O bond lengths are 2.088 Å, and the O−O bond length is 1.289 Å, while in $\mathbf{10}_{end}$, the Cu−O bond length is 1.964 Å, and the O−O bond length

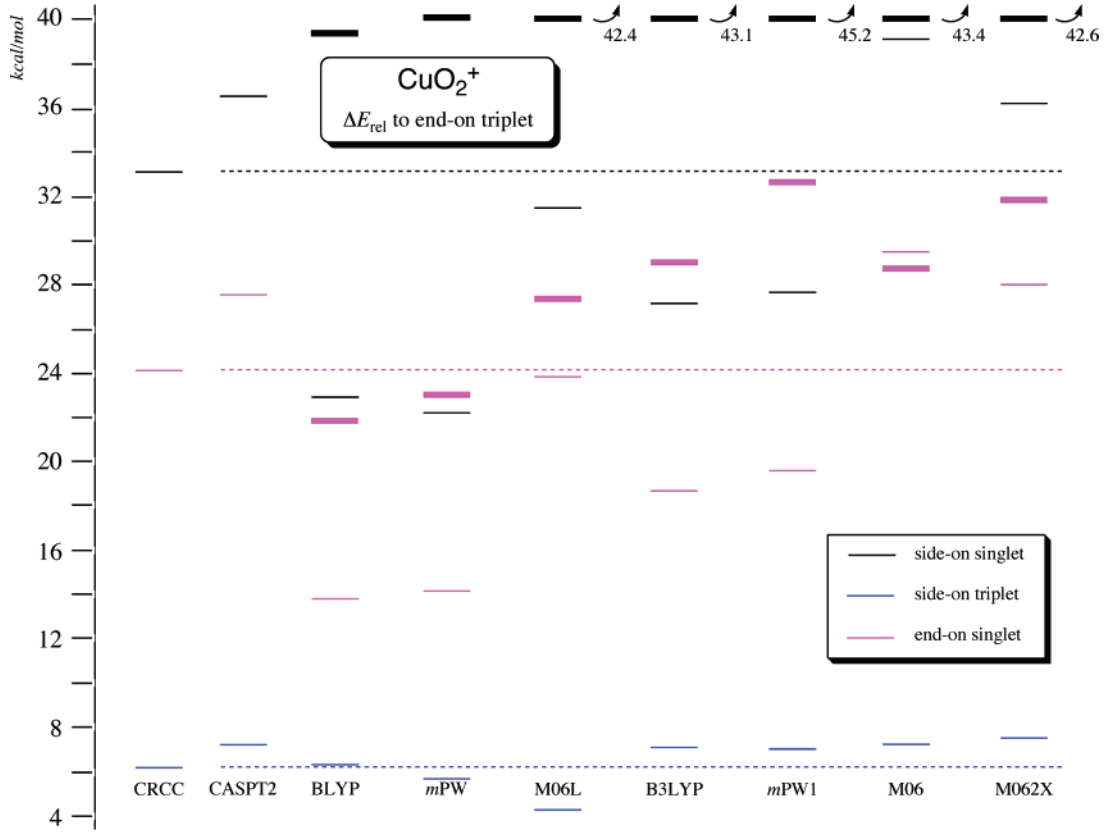

Figure 1. Comparison of different levels of theory to CR-CC(2,3) taken as a standard (dotted lines across the graph refer to this level). For DFT models, thicker lines refer to RDFT, while thinner lines refer to spDFT (raw BS DFT results are not shown).

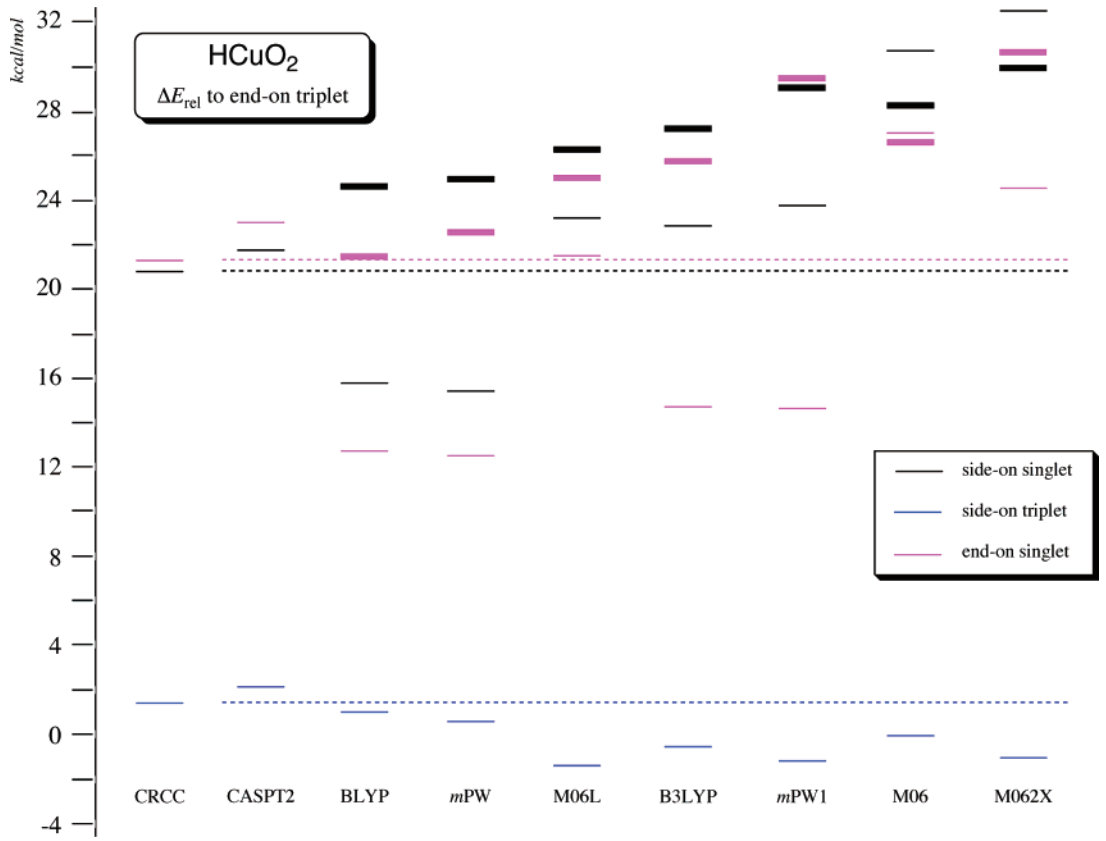

Figure 2. See caption to Figure 1.

is 1.309 Å. These geometric data are consistent with more Cu−O bonding and concomitant charge transfer in $\mathbf{10}_{end}$ than in $\mathbf{10}_{side}$. Energetic results are summarized in Figure 4, with raw data available in Table S-3 of the Supporting Information.

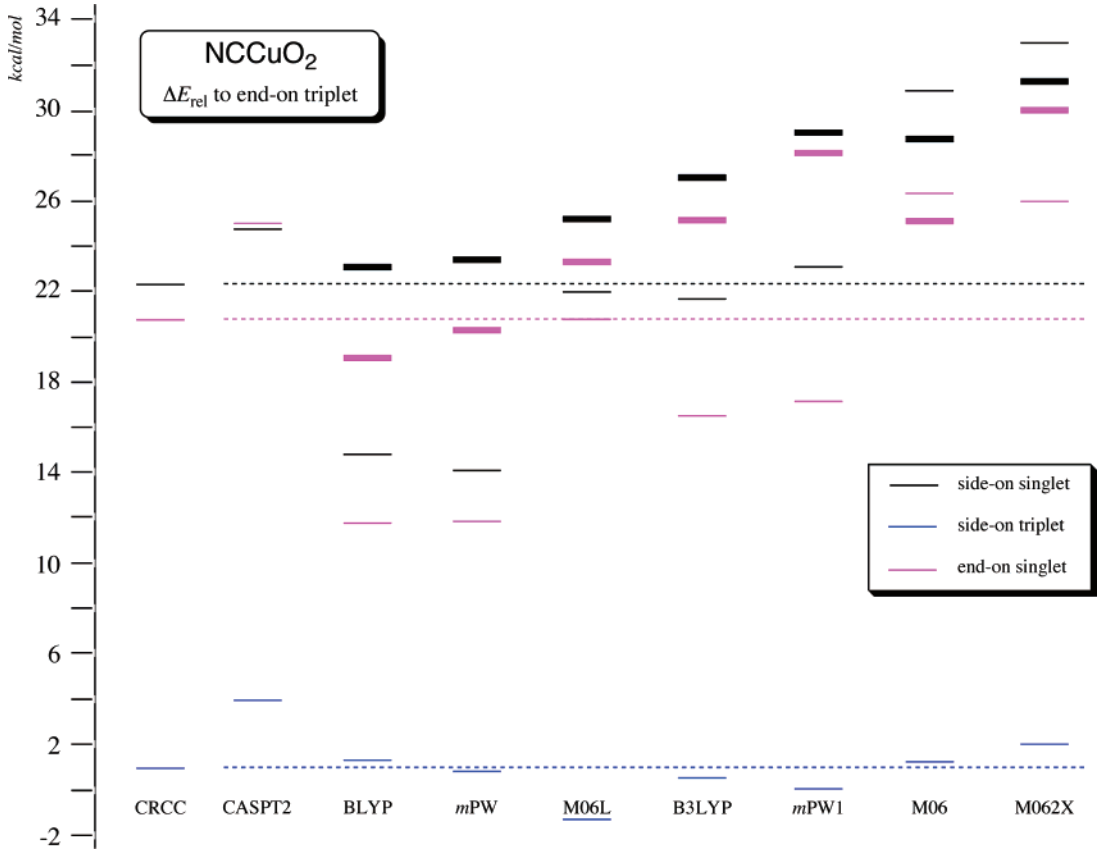

Figure 3. See caption to Figure 1.

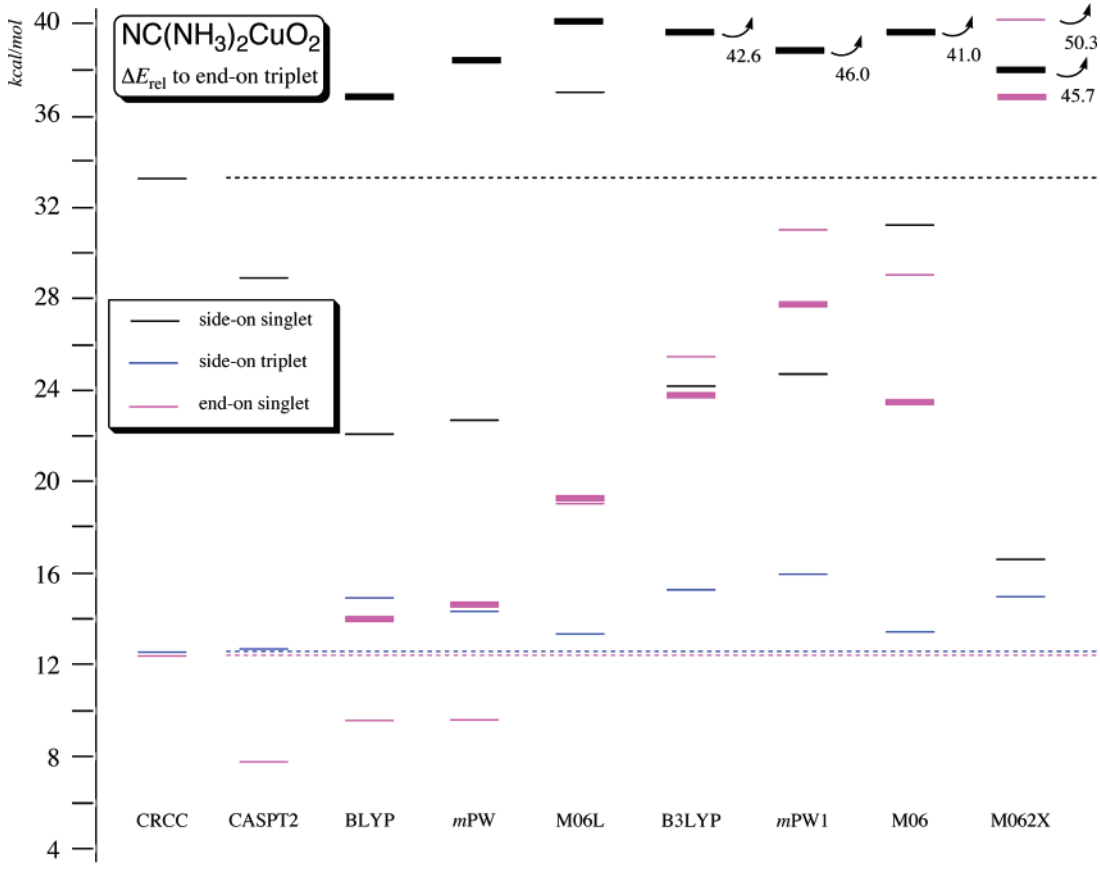

Figure 4. See caption to Figure 1.

In the case of **10**, CASPT2 predicts the singlet energies relative to the triplets to be lower than the results from the CR-CC(2,3) level, although there is quantitative agreement between the two levels for the triplets. The DFT levels provide fair to

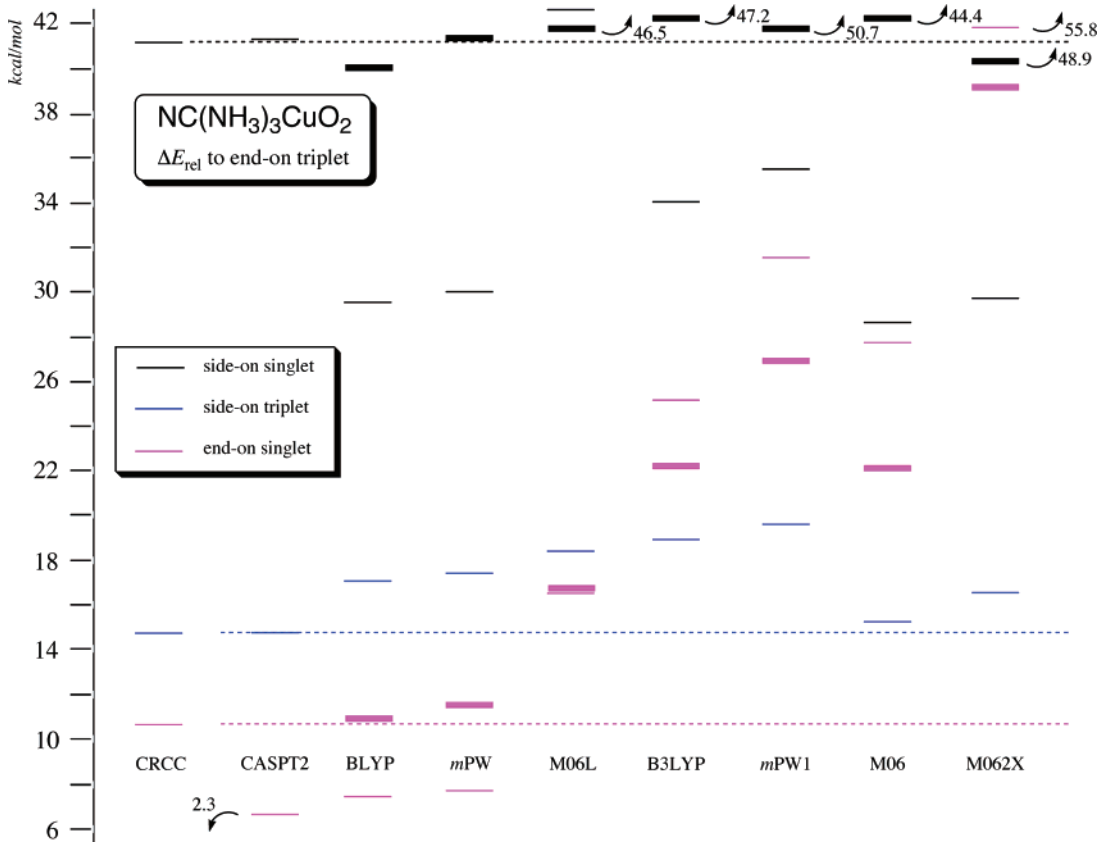

Figure 5. See caption to Figure 1.

good relative triplet energies but span ranges of 20 and 40 kcal mol^{-1}, respectively, in their sp predictions for the relative energies of the side-on and end-on singlets. The end-on singlet predictions are particularly sensitive to the amount of HF exchange in the functional, with this isomer predicted to increase dramatically in energy as more HF exchange is included. This sensitivity suggests substantial biradicaloid LCu(II)O_2(−) character in the electronic structure, which is entirely consistent with the geometric data for **10**$_{end}$.

$NC(NH_2)_3CuO_2$. To explore the effect of increasing the number of donating lone pairs around the Cu atom, we next examined **11**, whose set of ligands may be considered an anionic analogue for the tetradentate ligands present in **2** and **3**. In this case, both coordination geometries about Cu are trigonal bipyramidal as in **10**$_{side}$, with the proviso of course that the O_2 fragment is η^2 in **11**$_{side}$. Isomer **11**$_{side}$ has Cu−O bond lengths of 2.555 Å and an O−O bond length of 1.265 Å; these data reflect an obviously weak interaction. Isomer **11**$_{end}$, on the other hand, has a Cu−O bond length of 1.964 Å and an O−O bond length of 1.315 Å. The geometric details associated with the CuO_2 portions of **10**$_{end}$ and **11**$_{end}$ are thus very similar, and there is clearly much more Cu−O bonding and charge transfer in **11**$_{end}$ than in **11**$_{side}$. Energetic results are shown in Figure 5, and the numerical data are listed in Table S-4 of the Supporting Information.

As might be expected from the geometric analysis, all levels of theory predict the side-on isomers to now be higher in energy relative to their end-on analogues than was the case in **10**. The S−T splitting in **11**$_{end}$ favors the triplet by a slightly smaller margin than in **10**$_{end}$, a point to which we will return in the Discussion. The behavior of the DFT functionals with respect to predicting the relative isomer energetics in **11** is quite similar to that observed for **10**. We note in addition for **10** and **11** that while spM06L is subject to errors in predicted singlet relative energies of up to 6 kcal mol^{-1}, this is still substantially better than for any other functional surveyed here.

$(HCO_2)CuO_2$. We next examined **12**, where the formate ligand is itself bidentate. Geometrically, **12**$_{end}$ is characterized by a Cu−O bond length of 1.822 Å and an O−O bond of 1.280 Å, while **12**$_{side}$ has Cu−O bonds of 1.914 Å and an O−O bond length of 1.341 Å. There is a marked contrast, then, in the amount of bonding and charge transfer in **12**$_{side}$ as compared to the other side-on isomers thus far (cf. Table 1). This also can be seen in the relative isomer energies illustrated in Figure 6 (data in Table S-5 of the Supporting Information).

For the first time, the CR-CC(2,3) and CASPT2 levels predict the side-on isomers, singlet and triplet, to be lower than the end-on triplet. Moreover, the S−T splitting in **12**$_{side}$ is predicted to favor the triplet by only about 7−8 kcal mol^{-1}, a substantially smaller margin than in any of **7**−**11**. At the DFT levels of theory, it is now the side-on singlet relative energies that are most sensitive to the percent incorporation of HF exchange, suggesting that it is now this isomer that has a greater biradicaloid LCu(II)O_2(−) character. However, it is also true that in this case, the span of relative energy predictions made by the DFT models is smaller than in previous cases.

$(H_5C_3N_2)CuO_2$. We finally consider **13**, where the diketiminate ligand is again bidentate but is a stronger donor than formate. This is particularly evident in the geometrical data for **13**$_{side}$, where relative to **12**$_{side}$ the Cu−O bond length is shortened to 1.890 Å, and the O−O bond length extends to 1.366 Å (Table 1). The data for **13**$_{end}$, on the other hand, show a more modest charge transfer to O_2 (O−O bond length of 1.285 Å) in spite of a relatively short Cu−O bond length of 1.854 Å. Energetic data are again presented graphically in Figure 7, with data in Table S-6 of the Supporting Information. In this case, however, we take the side-on triplet as the relative zero of energy in Figure 7. The end-on triplet is predicted by the CASPT2 and M06L

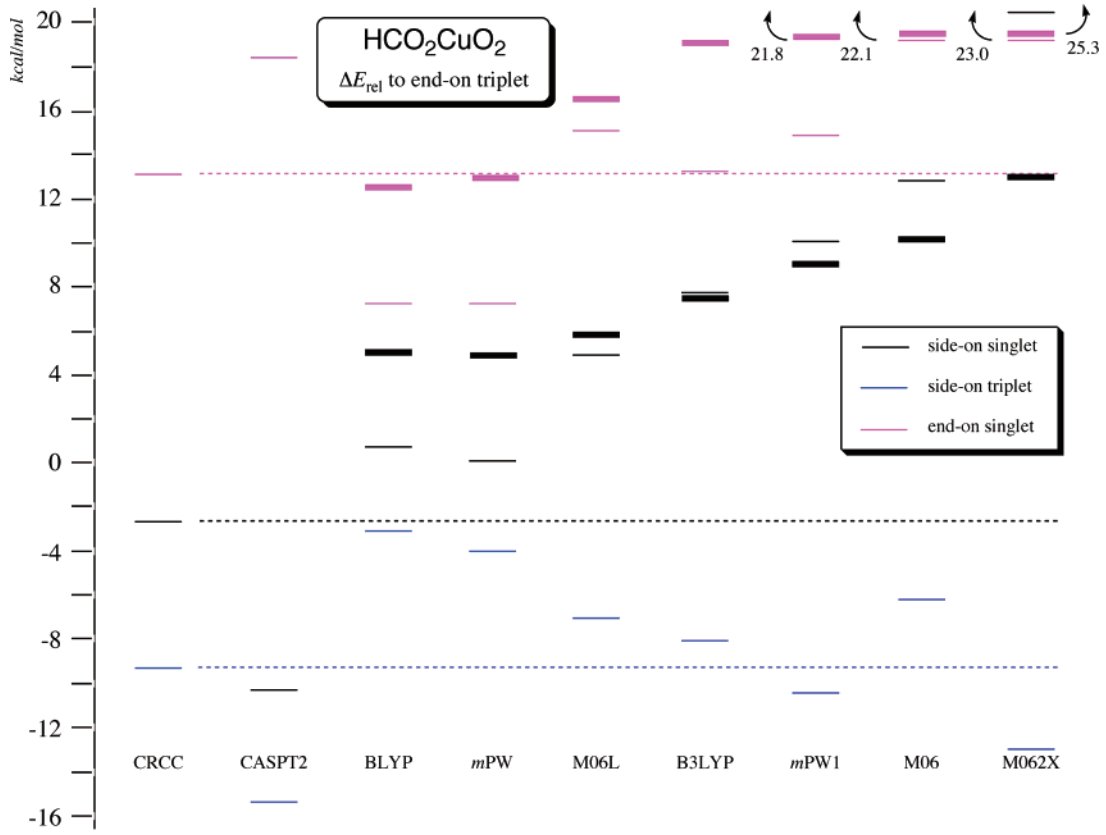

Figure 6. See caption to Figure 1.

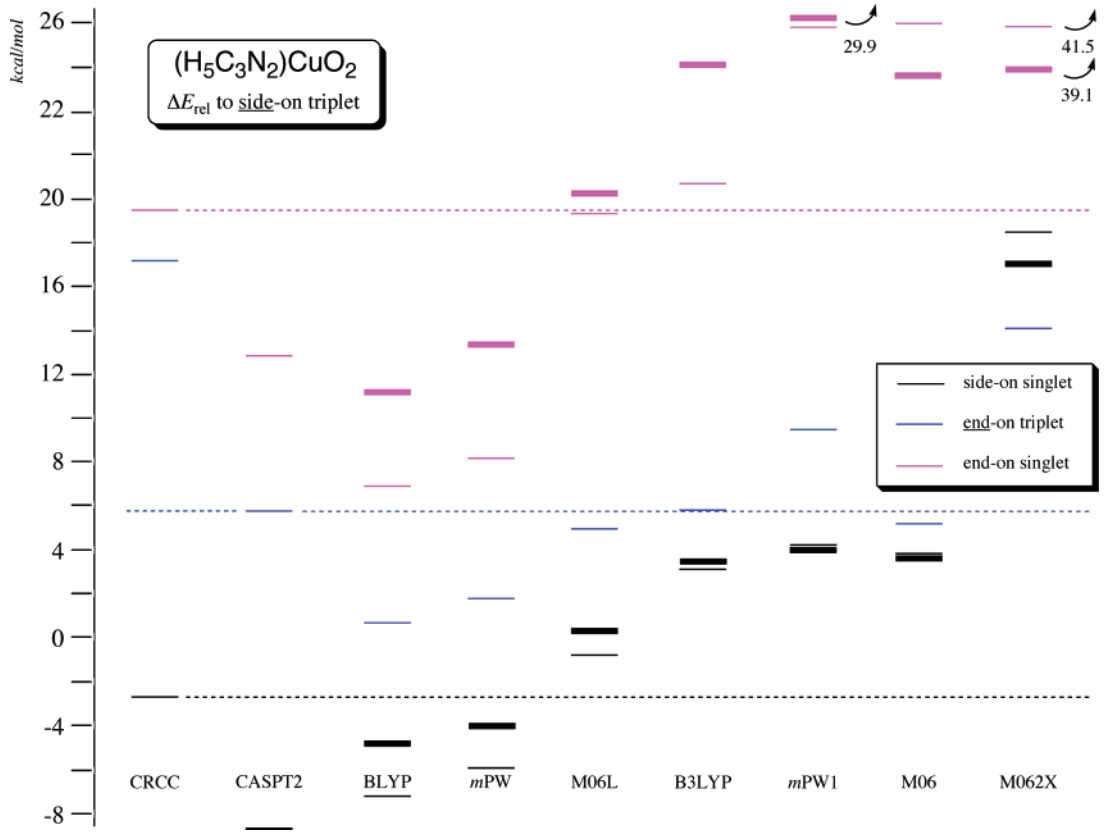

Figure 7. Comparison of different levels of theory to CR-CC(2,3), taken as a standard for the side-on and end-on singlet states, and CASPT2, taken as a standard for the end-on triplet state (dotted lines across the graph refer to CR-CC(2,3) for singlets and to CASPT2 for the end-on triplet, where the CR-CC(2,3) value is problematic). For DFT models, thicker lines refer to RDFT, while thinner lines refer to spDFT (raw BS DFT results are not shown).

levels to be about 6 kcal mol^{-1} higher in energy than the side-on triplet. As the triplets are well described by single determinantal wave functions, these predictions should be reasonably accurate (as they have been in general for **7**−**12**). Moreover,

this separation is roughly consistent with the triplet−triplet separation in **12**, which is electronically similar to **13**. Nevertheless, the CR-CC(2,3) level predicts the end-on triplet to be 17.3 kcal mol^{-1} higher in energy than the side-on triplet. We speculate that this is associated with a poor ROHF reference for the end-on triplet in the CR-CC calculation, although various attempts to find lower energy ROHF solutions that could lower the end-on triplet CR-CC(2,3) energy were not successful. In any case, if the end-on triplet is used as the zero of energy, the possibly anomalous behavior of the CR-CC(2,3) solution for this particular state masks the behavior of other models, while much more consistent results are obtained when the side-on triplet, correctly described by CR-CC(2,3), serves as the zero of energy (Figure 7).

As with **12**, the side-on isomers are predicted to be lower in energy than their end-on counterparts. And, for the first time, CR-CC(2,3), CASPT2, and the local spDFT models all predict the lowest energy side-on electronic state to be a singlet and not a triplet. The sensitivity of the relative singlet energies predicted by the DFT models to inclusion of HF exchange in the functionals is quite high for both singlets. The quantitative accuracy of the spM06L functional stands out as compared to the others.

Discussion

As with experimentally characterized compounds **1**−**6**, the computationally characterized $LCuO_2$ species **7**−**13** show a large range of preferences for geometry, charge transfer, and spin-state preference. We next describe an orbital-based approach for explaining these phenomena and close with some discussion of the implications for future modeling efforts.

Stereoelectronic Analysis. In the absence of ligands, the interaction of Cu(I) with molecular O_2 involves a closed-shell d^{10} metal atom with a triplet diatomic. The second ionization potential of Cu is 20.29 eV, while the electron affinity of O_2 is 0.45 eV,[101] so one may regard the separation between the quintuply degenerate highest occupied molecular orbitals (HOMOs) of Cu and the doubly degenerate singly occupied π^* acceptor orbitals of O_2 as being very large indeed. As such, any interaction between these two species, in the absence of ligation, should be primarily electrostatic in nature. This is entirely consistent with the computed results for **7**, which suggest an ion−dipole complex character for the cluster. As the polarizability of O_2 is greater along the molecular axis than orthogonal to it,[102] an end-on geometry can be rationalized on a purely electrostatic basis. As there is little to no orbital hybridization between the two fragments, a triplet ground state with a S−T splitting similar to that of molecular O_2 also is expected, and our best CR-CC(2,3) and CASPT2 calculations confirm this.

Considering ligands, now, within the context of their effect on the Cu d orbitals, we have essentially two disparate sets in compounds **8**−**13**. If we define the *z*-axis as the axis from Cu to O in end-on geometries, and from Cu to the O−O midpoint in side-on geometries, and the *xz* plane as the plane containing Cu and the two O atoms in side-on geometries, then we may say that structures **8**−**11** have ligand donor lone pairs arrayed in such a way as to selectively destabilize the d_{z^2} orbital, while structures **12** and **13**, by virtue of their bidentate character, selectively destabilize the d_{xz} orbital. Figures 8 and 9, respectively, illustrate in an idealized fashion the degree to which these contrasting situations foster corresponding preferences for end-on and side-on coordination of the O_2 molecule, which is precisely what is observed computationally.

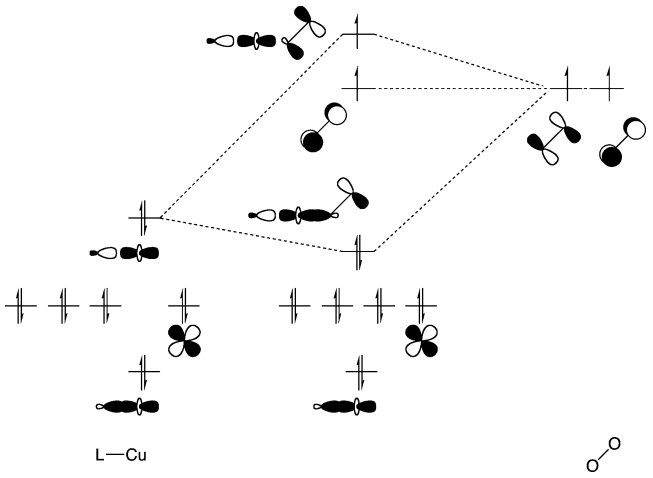

Figure 8. Perturbational molecular orbital diagram for the end-on interaction of LCu with O_2, which is favored for a ligand (or ligands) L that selectively destabilizes a d_{z^2} orbital hybrid by axial or equatorial disposition (e.g., systems **8**−**11**). For the sake of simplicity, O_2 σ orbitals are not included in this diagram, but they do play a role in polarizing the illustrated interactions.

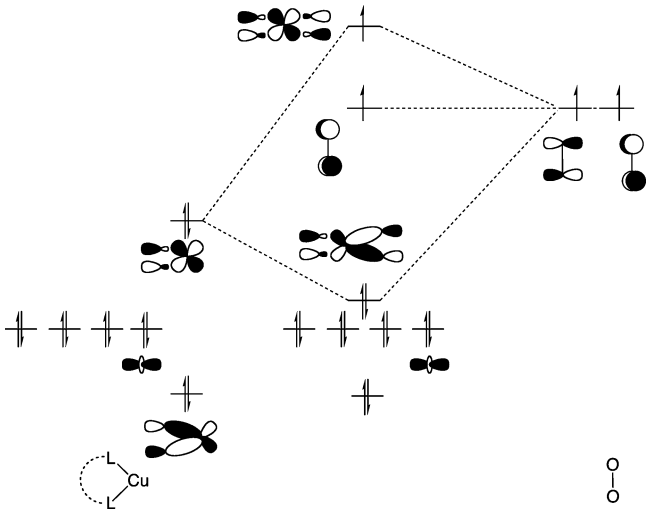

Figure 9. Perturbational molecular orbital diagram for the side-on interaction of LCu with O_2, which is favored for a ligand (or ligands) L that selectively destabilizes a d_{xz} orbital hybrid by, for example, bidentate disposition, as in systems **12** and **13**.

In the end-on case illustrated in Figure 8, the d_{z^2} hybrid, which becomes the HOMO through a destabilizing four-electron interaction between the d orbital and the L lone pair, has σ character and thus cannot interact with both lobes of the in-plane O_2 π^*. Instead, an end-on geometry is adopted (with a Cu−O−O bond angle in excess of 90° owing to other electrostatic interactions beyond those shown in the diagram, which uses highly idealized orbital shapes for purely schematic purposes). In Figure 8, the electronic state after orbital mixing remains a triplet. It is evident, however, that further increasing the energy of the initial d_{z^2} hybrid HOMO should lead to increased mixing with the in-plane O_2 π^*, and such mixing should raise the energy of the antibonding hybrid (the highest energy orbital in the diagram) to the point where the energy gain associated with demotion of the electron to the lower energy out-of-plane O_2 π^* exceeds the additional repulsion associated with spin-pairing, and a singlet state will result. To achieve this increase in the d_{z^2} hybrid HOMO, either stronger donor ligands L, or more of them (appropriately distributed to interact with d_{z^2}), or both, are required. This is consistent with the steady decrease in the energy of the singlet state relative to the triplet

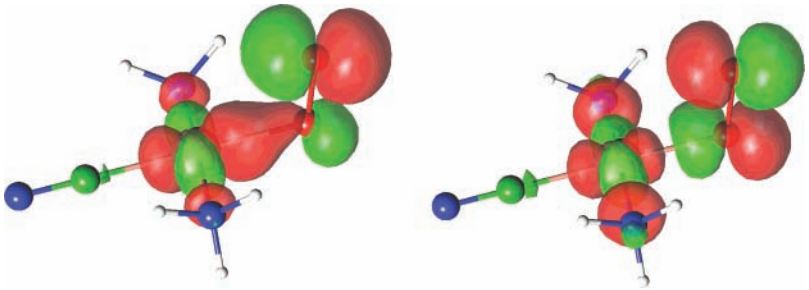

Figure 10. MCSCF MOs for singlet $\mathbf{10}_{end}$ from mixing of Cu d_{z^2} and O_2 in-plane π^* orbitals.

as we go from $\mathbf{8}_{end}$ to $\mathbf{9}_{end}$, $\mathbf{10}_{end}$, and $\mathbf{11}_{end}$: from 21.5 to 20.8, 12.3, and 10.7 kcal mol^{-1} at the CR-CC(2,3) level. Even with the tetradentate ligand set $NC(NH_3)_3$, the triplet remains the ground state by a sizable margin, suggesting that the energy splitting between the two O_2 π^* orbitals is not yet very large. This can be attributed to the σ nature of the d_{z^2} orbital, which can overlap with only one-half of the orbital amplitude of the in-plane O_2 π^*; this reduced total overlap causes the degree of mixing to be damped since mixing depends on both energy separation and overlap.[103]

As the singlet state becomes closer in energy to the ground state in **8**−**11**, it also develops substantial biradical character, consistent with a $LCu(II)O_2(-)$ valence bond formulation. This is most readily seen in the relevant MCSCF wave functions. The percentages of the two dominant configurations in the wave functions for singlets $\mathbf{8}_{end}$, $\mathbf{9}_{end}$, $\mathbf{10}_{end}$, and $\mathbf{11}_{end}$ are 94/6, 94/6, 73/27, and 67/33, respectively. As a result, two molecular orbitals have occupation numbers differing substantially from zero or two in singlet $\mathbf{10}_{end}$ and $\mathbf{11}_{end}$; these orbitals are illustrated in Figure 10 for $\mathbf{10}_{end}$. It is apparent that the orbitals represent bonding and antibonding combinations of the Cu d_{z^2} and in-plane O_2 π^*, exactly as illustrated in Figure 8. Positive and negative linear combinations of these two orbitals can be taken to generate either the pure Cu d_{z^2} or the O_2 π^* orbital, and in the limit of a 50/50 weighting of the dominant MCSCF configurations, a pure biradical resonance structure would be appropriate. In the case of the orbitals in Figure 10, the MCSCF occupation numbers are 1.47 and 0.56, corresponding to substantial but not complete biradical character. Nevertheless, this indicates a substantial challenge for the single-reference theoretical models.

In the case of side-on O_2 coordination, summarized in Figure 9, the situation is quite similar to that discussed previously, except that the destabilized d_{xz} orbital is able to overlap with the entirety of the in-plane O_2 π^* orbital to form two σ-like interactions. As such, perturbations associated with ligand(s) can provide more tuning influence, so that the requisite separation in O_2 π^* orbitals necessary to generate a singlet ground state can be achieved. Thus, while formate as a ligand fosters a preference for side-on coordination, $\mathbf{12}_{side}$ remains a ground-state triplet by 7 kcal mol^{-1} at the CR-CC(2,3) level. The stronger diketiminate donor, on the other hand, is sufficient to cause $\mathbf{13}_{side}$ to have a singlet ground state predicted to be 2.6 kcal mol^{-1} below the triplet at the CR-CC(2,3) level.

Visualizations of the full sets of frontier orbitals in **8**−**13** are entirely consistent with the above analyses. In the interest of brevity, we do not include pictures of all of the individual orbitals here, distilling their content instead into Figures 8−10. We note that other Cu d orbitals can and do overlap with appropriate O_2 fragment orbitals; however, these interactions tend to do little to differentiate between end-on and side-on geometries because a combination of larger energy separations and smaller overlaps (of π and δ character) makes them much less energetically important.

Our analysis is consistent with results previously reported by Bérces,[104] who studied $LCuO_2^+$ with L being the tridentate 1,4,7-triazacyclononane (TACN) ligand at the BP86 density functional level. Bérces noted that the coordination of the TACN ligand varied depending on whether the O_2 fragment was coordinated in an end-on or side-on fashion. In particular, the end-on geometry was distorted significantly from tetrahedral so as to place the nitrogen donor atoms in positions similar to those adopted by the CN and two NH_3 nitrogen atoms in **10** (i.e., so as best to mimic the orbital interaction diagram in Figure 8). By contrast, in the side-on isomer, two nitrogen atoms were nicely placed to overlap with the d_{xz} orbital as illustrated in Figure 9 (in positions similar to those adopted by the nitrogen atoms in system **13**), while the third nitrogen was more loosely coordinated at a distance of 2.25 Å. Other geometric parameters were similar to those reported here for analogous geometries.

Thus, given a rigid, multidentate ligand, a simple geometric analysis together with the orbital interaction model given in Figures 8 and 9, which is consistent with the results of the most accurate CR-CC(2,3) calculations, provides a prescription for predicting end-on versus side-on geometric preferences, and the nature of the electronic ground state depends on the electron-donating strength of the ligand(s), with a greater influence being required to generate an end-on singlet as compared to a side-on singlet. Returning to structures **1**−**6**, we see that **2** and **3** have relatively rigid geometries such as those studied for **11**, and end-on bonding is favored, as expected. The triplet ground state of **2** and the rough similarity of the ligands in **2** and **3** suggest that **3** as well might be expected either to have a triplet ground state or to have at best a very small preference for the singlet. The PAM active site, **1**, is potentially more plastic as the ligands are different amino acid residues. Indeed, the coordination of the ligands about the metal atom is roughly tetrahedral.[19] This observation, coupled with the very short O−O bond, suggests a situation more analogous to computational model **7**, i.e., negligible Cu−O bonding owing to weak donors, a resultant preference for an end-on geometry, and an almost certain triplet ground state.

As for **5** and **6**, even the unsubstituted diketiminate ligand in **13** is sufficient to make the side-on singlet the preferred state, and the additional donating power associated with substituents in the experimental systems would only be expected to enhance this preference, consistent with observed geometries and spin states. The nature of the tris(pyrazoloborate) is such that it, like the side-on TACN example discussed above, has short in-plane Cu−N distances of 1.99(2) Å and one considerably longer pseudo-axial Cu−N distance of 2.25(2) Å. Moreover, the in-plane N−Cu−N bite angle is 93(1)°, making this system resemble computational model **13** in most respects. The weaker donating ability of the tris(pyrazoloborate) ligand as compared

to diketiminate is consistent with the reduced degree of charge transfer observed and suggests that the S−T splitting (which has not been measured for **4**) should be smaller than those for **5** and **6**.

We note that our above analysis should not be regarded as being in conflict with standard preferences well established in copper coordination chemistry (e.g., that Cu(I), Cu(II), and Cu(III) complexes have general preferences for tetrahedral, tetragonal, and square-planar geometries, respectively, when coordinated by four ligands). Indeed, such preferences (which are themselves orbital-based) have been used to good effect in explaining the structural preferences of di-copper-O_2 species supported by different ligands.[46,105] A key feature of O_2 as a ligand, however, is the degree to which covalency may influence Cu−O bonding, and this adds an additional factor to consider when assessing preferred $LCuO_2$ geometries and electronic spin states.

Implications for Modeling. We have taken the CR-CC(2,3) model here as our standard with respect to energetic predictions. We base this in part on our prior work on $(LCu)_2O_2$ systems,[50,51] where the convergence of CR-CC(2,3) predictions and their comparison to multireference configuration interaction results and relevant experimental data suggested the model to be robust and quantitatively useful. The results of the CR-CC(2,3) calculations reported in the present study are consistent with the end-on/side-on and singlet/triplet preferences resulting from orbital analysis shown in Figures 8 and 9, reinforcing our belief in the ability of the CR-CC(2,3) scheme to provide accurate energetic predictions. In the present systems, there is moreover a generally good agreement between CR-CC(2,3) and CASPT2, with the exception of triplet $\mathbf{13}_{end}$ noted above, where we experienced difficulties in identifying the appropriate ROHF reference determinant for the CR-CC(2,3) calculations. This was not true in the $(LCu)_2O_2$ cases[49−51] and reflects the difference in active space requirements for the CASPT2 level of theory when only a single metal atom is present instead of two. In practice, we find that a balanced active space for a CASSCF $LCu(I)O_2$ wave function should include all of the oxygen p functions and two sets of copper d functions, which amounts to 16 orbitals occupied by 18 electrons (10 3d electrons for Cu(I) and 4 2p electrons from each O atom). Such an (18,16) active space is just within the practical limitations on a typical CASSCF calculation (in certain instances, we also found that one occupied orbital could be removed from the active space, i.e., generating a (16,15) space, because the particular ligand environment rendered it so nearly doubly occupied in all states that it simply added instability to the CASSCF convergence when it was included) and appears to have been useful based on the results reported above. Thus, we consider agreement between CR-CC(2,3) and CASPT2 to further establish the quantitative utility of the former as a benchmark level against which we now proceed to assess the quality of various DFT protocols. The single-reference black-box nature of the CR-CC(2,3) approach, which relies on the standard RHF and ROHF references, should be emphasized in this context as well since it greatly facilitates the calculations in cases where the adequate choice of active orbitals for multireference calculations, such as CASPT2, becomes problematic, as observed in the $(LCu)_2O_2$ systems.[50−52]

To provide a quantitative gauge of the performance of a given theoretical model relative to CR-CC(2,3), we examine five error measures. First, we consider the energies of end-on singlets, side-on triplets, and side-on singlets relative to their respective end-on triplets, and in Table 3 we report the mean unsigned error (MUE) and maximum absolute error (MAE) in these predicted relative energies for **7**−**13** for all of the theories examined here. This measure of error, however, may be considered to be biased by the accuracy of the end-on triplet calculations (which case is indeed in question for $\mathbf{13}_{end}$, so that Table 3 actually takes the side-on triplet as the relative zero of energy for compound **13** and uses the CASPT2 energy for $\mathbf{13}_{end}$ relative to $\mathbf{13}_{side}$ as the standard for computing errors). A potentially more balanced approach is to consider the S−T splittings for the side-on and end-on structures and the relative singlet−singlet and triplet−triplet energy differences between the two structures. Table 3 also presents the MUEs and MAEs in these predicted energies as compared to CR-CC(2,3) for **7**−**13** for all of the theories examined here (noting, again, that whenever $\mathbf{13}_{end}$ is involved in an energy difference, it is the CASPT2 prediction that is taken as the standard). Finally, as an overall quality indicator, *Q*, we arbitrarily took the product of the MUE and MAE values characterizing the S−T splittings and the relative singlet−singlet and triplet−triplet energy differences (i.e., those just detailed and listed in the third- and second-to-last columns in Table 3), divided by 100, and listed these values in the final column of Table 3. Thus, the lower the value of *Q*, the more accurate the method, and a single large outlier will be balanced if there is still overall a very small MUE.

TABLE 3: Mean Unsigned and Maximum Absolute Errors (kcal mol^{-1}) and Their Product for Different Theoretical Levels

	E_{rel}[a]		ΔE[b]		
level of theory	MUE	MAE	MUE	MAE	Q[c]
R(O)HF	39.9	100.5	31.8	100.5	32.0
CCSD	7.7	20.3	6.4	20.3	1.3
CR-CC(2,3)	0.5	11.5	0.6	11.5	0.1
CAS(18,16)	8.9	31.2	9.3	31.2	2.9
CASPT2(18,16)	2.9	8.4	2.5	8.5	0.2
RBLYP[b]	2.8	8.3	2.8	8.6	0.2
UBLYP	8.8	18.6	8.2	20.4	1.7
spBLYP	8.9	12.9	5.6	14.1	0.8
R*m*PW	2.6	7.3	2.7	7.6	0.2
U*m*PW	8.7	19.2	8.0	20.4	1.6
sp*m*PW	8.7	11.5	5.4	14.1	0.8
RM06L	3.9	9.3	3.7	10.8	0.4
UM06L	5.7	15.0	5.3	14.2	0.7
spM06L	4.9	7.6	2.7	7.0	0.2
RB3LYP	5.4	11.7	4.7	11.7	0.6
UB3LYP	7.0	16.2	7.5	19.3	1.5
spB3LYP	6.8	14.6	6.6	22.4	1.5
R*m*PW1	7.7	16.3	6.4	16.3	1.0
U*m*PW1	7.3	16.0	8.2	21.5	1.8
sp*m*PW1	7.7	21.1	8.1	27.3	2.2
RM06	5.2	12.7	5.1	11.4	0.6
UM06	5.1	12.7	6.0	19.2	1.2
spM06	7.1	17.3	7.3	29.9	2.2
RM06-2X	10.2	28.6	9.0	28.6	2.6
UM06-2X	8.4	21.7	10.1	33.3	3.4
spM06-2X	11.4	45.2	14.0	56.8	7.9

[a] End-on singlet and side-on singlet and triplet energies relative to end-on triplet for **7**−**13** as compared to CR-CC(2,3) values, except for **13** where the side-on triplet was taken as the relative zero of energy; standard energy for $\mathbf{13}_{end}$ relative to $\mathbf{13}_{side}$ was taken from the CASPT2 level. [b] S−T splittings for side-on and end-on isomers and singlet−singlet and triplet−triplet energy differences between isomers. [c] Product of preceding two columns divided by 100.

As expected, CR-CC(2,3) gives the smallest value of *Q* (0.1); indeed, were it not for the anomalous CR-CC(2,3) value for $\mathbf{13}_{end}$, *Q* would necessarily be zero for our standard level of theory. There are four levels of theory that have *Q* values of 0.2, the next lowest value after that for CR-CC(2,3). One of these is CASPT2, whose generally good agreement with CR-

CC(2,3) we have already noted and used as a basis for our confidence in the model. Another is the spin-purified M06L density functional level. This is also a result that increases our confidence in the agreeing models since M06L has been carefully parametrized against extensive sets of experimental data,[62,65] it is a local functional (and experience suggests that including HF exchange introduces serious errors in predicted state-energy splittings between high- and low-spin states for analogous dicopper systems),[50,51,106] and the spin-purification procedure provides a practical method for dealing with unstable restricted KS wave functions.

Fascinatingly, the BLYP and *m*PW density functionals are also predicted to have *Q* values of 0.2 when a restricted formalism is used to compute singlet energies. These two functionals are the remaining local functionals among those tested. Considering the same restricted protocol for singlet energies, M06L has a *Q* value of 0.4, which is twice the error of the spin-purified approach but still among the lower *Q* values in Table 3. Thus, there seems to be some utility to the restricted pure functional approach for **7**−**13**, although a more in-depth understanding of this phenomenon is beyond the scope of the present work. It is worth noting that converging the restricted singlet wave functions tends to be somewhat difficult (standard convergence schemes generally fail, and a resort to slower quadratically convergent algorithms is nearly always required), so the protocol is not as practical as spin-purified M06L, but it may be worth studying to gain insight into functional behavior in biradical situations.

Amplifying this point, we note that there tends to be confusion in the literature with respect to the use of restricted DFT to model a potential singlet biradical. Thus, for example, one may find authors discarding the use of certain functionals if they fail to break symmetry because of a belief that an accurate treatment *requires* symmetry breaking. However, this is not true. In formal DFT, this issue is related to the v-representability of the density for these cases, that is, the ability to represent the exact density with a single, restricted Slater determinant. The exact density for a singlet has zero spin density at all spatial positions, and an unrestricted broken-symmetry KS determinant violates this requirement—thus, were a restricted solution to be available, it would be more consistent with the singlet nature of the wave function. The issue of exactly which densities are v-representable remains unsolved in formal DFT. However, Schipper et al.[107] have shown that restricted single-determinantal KS wave functions can indeed well represent the exact density (as determined from large MRCI calculations) even in systems with substantial singlet biradical character such as methylene and C_2. In the case of the $LCuO_2$ systems studied here, we do not have access to the exact densities, so we cannot make a similar comparison, but the quality of the predicted energies suggests that the utility of restricted DFT (with pure functionals) when applied to singlet biradicals should not be automatically discounted.

For none of the functionals is the use of raw unrestricted broken-symmetry singlet energies a good option. In the case of the pure functionals, spin purification improves the functional's *Q* value; for B3LYP, the *Q* value is unchanged after spin purification, and for the hybrid functionals incorporating still more exact HF exchange, spin purification *increases* the *Q* value, suggesting that errors introduced by inclusion of HF exchange are amplified by the spin-purification procedure. Using the restricted singlet energies is the best option for all of the hybrid functionals, but even for the best, B3LYP, the value of *Q* is a rather large 0.6 and large MAEs are observed.

We note that the basis set we employed for energy calculations is of polarized triple-ζ quality. DFT predictions such as those undertaken here tend to be well converged with such basis sets.[40] Thus, given the generally good agreements between M06L, CR-CC(2,3), and CASPT2 presented above, we presume that the predictions for model systems **7**−**13** are likely to be converged to within 1 or 2 kcal mol^{-1}. However, these model systems are not likely amenable to experimental study—they are useful primarily for illustrating fundamental changes in electronic structure associated with ligands and coordination geometries.

From this study, we postulate that future modeling efforts focusing on $LCuO_2$ and related systems may profitably use the M06L functional with spin purification as an efficient means to compute energies for alternative geometries and spin states. The generally good performance of most density functionals for geometries is already quite well established.[40] We also conclude that when robust, high-accuracy results for $LCuO_2$ and analogous systems are desired, the CASPT2 and CR-CC(2,3) models will be excellent options provided the necessary computational resources are available. Currently, the CR-CC(2,3) method can be routinely applied to systems with up to about 80−100 correlated electrons, such as those studied in the present and earlier work,[50,51] but this situation should improve once low-order scaling variants of the CR-CC(2,3) approach employing localized orbitals and parallel code development are available; progress on both of these fronts is proceeding.

Conclusion

Good agreement between highly correlated levels of single- and multiconfigurational wave function theories and local density functional theories for the relative energies of different spin states and coordination motifs of $LCuO_2$ models permits the analysis of essential factors influencing structure and electronic ground state. When one or more ligands are bound to Cu in a fashion that, by filled-orbital−filled-orbital overlap, destabilizes the Cu d_{z^2} orbital, a preference for end-on binding of O_2 is observed. In such a case, a triplet ground state is expected unless the ligands are very strongly donating, as resonance between the Cu d_{z^2} orbital and in-plane O_2 π^* orbital is reduced by modest overlap, making it more difficult to achieve significant separation in the frontier orbitals. By contrast, a much better overlap between the Cu d_{xz} orbital and the in-plane O_2 π^* orbital is available for a side-on coordination motif, and this becomes favored when a ligand or ligands are bound so as to raise the energy of the Cu d_{xz} orbital. This greater resonance leads to more oxidative charge transfer and more ready access to a singlet ground state. Thus, varying ligand coordination schemes and donating power, it is possible to rationalize a continuum of species from $LCu(I)O_2$, to $LCu(II)O_2(-)$, to $LCu(III)O_2(2-)$. Because of the significant biradical character that develops in the $LCu(II)O_2(-)$ region of this continuum, theoretical models must be able to handle multideterminantal character in relevant wave functions to be quantitatively useful. This study demonstrates that the spin-purified M06L density functional level, the recently developed size extensive completely renormalized coupled-cluster method with singles, doubles, and non-iterative triples, CR-CC(2,3), and multiconfigurational second-order perturbation theory all provide descriptions consistent with one another for the full variety of $LCuO_2$ motifs, including biradical $LCu(II)O_2(-)$ formulations. Such mutual consistency between two different many-body methods and a well-benchmarked DFT model employing a

polarized triple-ζ basis set also enhances confidence in the quantitative accuracy of the theoretical models applied to such molecules.

Acknowledgment. This work was supported by the U.S. National Science Foundation (CHE-0610183 to C.J.C. and Graduate Research Fellowship to J.R.G.), the Swiss National Science Foundation (200021-111645/1 to L.G.), the Chemical Sciences, Geosciences, and Biosciences Division, Office of Basic Energy Sciences, Office of Science, U.S. Department of Energy (Grant DE-FG02-01ER15228 to P.P.), the High Performance Computing Center at Michigan State University, and the Minnesota Supercomputing Institute.

Supporting Information Available: Tables of absolute and relative electronic energies for all states and geometries of **8**−**13**, dominant MCSCF configurations, MO occupation numbers, Mulliken atomic partial charges, and software details. This material is available free of charge via the Internet at http://pubs.acs.org.

References and Notes

(1) Lewis, E. A.; Tolman, W. B. *Chem. Rev.* **2004**, *104*, 1047.
(2) Punniyamurthy, T.; Velusamy, S.; Iqbal, J. *Chem. Rev.* **2005**, *105*, 2329.
(3) Isabel, B.; Carrondo, M. A.; Peter, F. L. *J. Biol. Inorg. Chem.* **2006**, *11*, 539.
(4) Itoh, S. *Curr. Opin. Chem. Biol.* **2006**, *10*, 115.
(5) Klinman, J. P. *J. Biol. Chem.* **2006**, *281*, 3013.
(6) Smirnov, V. V.; Brinkley, D. W.; Lanci, M. P.; Karlin, K. D.; Roth, J. P. *J. Mol. Catal. A: Chem.* **2006**, *251*, 100.
(7) Bollinger, J. M.; Krebs, C. *Curr. Opin. Chem. Biol.* **2007**, *11*, 151.
(8) Cramer, C. J.; Tolman, W. B. *Acc. Chem. Res.* **2007**, *40*, 601.
(9) Fujisawa, K.; Tanaka, M.; Moro-oka, Y.; Kitajima, N. *J. Am. Chem. Soc.* **1994**, *116*, 12079.
(10) Aboelella, N. W.; Lewis, E. A.; Reynolds, A. M.; Brennessel, W. W.; Cramer, C. J.; Tolman, W. B. *J. Am. Chem. Soc.* **2002**, *124*, 10660.
(11) Cramer, C. J.; Tolman, W. B.; Theopold, K. H.; Rheingold, A. L. *Proc. Natl. Acad. Sci. U.S.A.* **2003**, *100*, 3635.
(12) Chen, P.; Root, D. E.; Campochiaro, C.; Fujisawa, K.; Solomon, E. I. *J. Am. Chem. Soc.* **2003**, *125*, 466.
(13) Jazdzewski, B. A.; Reynolds, A. M.; Holland, P. L.; Young, V. G.; Kaderli, S.; Zuberbuhler, A. D.; Tolman, W. B. *J. Biol. Inorg. Chem.* **2003**, *8*, 381.
(14) Aboelella, N. W.; Kryatov, S.; Gherman, B. F.; Brennessel, W. W.; Young, V. G.; Sarangi, R.; Rybak-Akimova, E.; Hodgson, K. O.; Hedman, B.; Solomon, E. I.; Cramer, C. J.; Tolman, W. B. *J. Am. Chem. Soc.* **2004**, *126*, 16896.
(15) Chen, P.; Solomon, E. I. *J. Am. Chem. Soc.* **2004**, *126*, 4991.
(16) Gherman, B. F.; Cramer, C. J. *Inorg. Chem.* **2004**, *43*, 7281.
(17) Hatcher, L. Q.; Karlin, K. D. *J. Biol. Inorg. Chem.* **2004**, *9*, 669.
(18) Mirica, L. M.; Ottenwaelder, X.; Stack, T. D. P. *Chem. Rev.* **2004**, *104*, 1013.
(19) Prigge, S. T.; Eipper, B. A.; Mains, R. E.; Amzel, L. M. *Science (Washington, DC, U.S.)* **2004**, *304*, 864.
(20) Schatz, M.; Raab, V.; Foxon, S. P.; Brehm, G.; Schneider, S.; Reiher, M.; Holthausen, M. C.; Sundermeyer, J.; Schindler, S. *Angew. Chem., Int. Ed.* **2004**, *43*, 4360.
(21) Kamachi, T.; Kihara, N.; Shiota, Y.; Yoshizawa, K. *Inorg. Chem.* **2005**, *44*, 4226.
(22) Kinsinger, C. R.; Gherman, B. F.; Gagliardi, L.; Cramer, C. J. *J. Biol. Inorg. Chem.* **2005**, *10*, 778.
(23) Reynolds, A. M.; Gherman, B. F.; Cramer, C. J.; Tolman, W. B. *Inorg. Chem.* **2005**, *44*, 6989.
(24) Reynolds, A. M.; Lewis, E. A.; Aboelella, N. W.; Tolman, W. B. *Chem. Commun. (Cambridge, U.K.)* **2005**, 2014.
(25) Aboelella, N. W.; Gherman, B. F.; Hill, L. M. R.; York, J. T.; Holm, N.; Young, V. G.; Cramer, C. J.; Tolman, W. B. *J. Am. Chem. Soc.* **2006**, *128*, 3445.
(26) de la Lande, A.; Gerard, H.; Moliner, V.; Izzet, G.; Reinaud, O.; Parisel, O. *J. Biol. Inorg. Chem.* **2006**, *11*, 593.
(27) Gherman, B. F.; Heppner, D. E.; Tolman, W. B.; Cramer, C. J. *J. Biol. Inorg. Chem.* **2006**, *11*, 197.
(28) Gherman, B. F.; Tolman, W. B.; Cramer, C. J. *J. Comput. Chem.* **2006**, *27*, 1950.
(29) Heppner, D. E.; Gherman, B. F.; Tolman, W. B.; Cramer, C. J. *Dalton Trans.* **2006**, 4773.
(30) Hill, L. M. R.; Gherman, B. F.; Aboelella, N. W.; Cramer, C. J.; Tolman, W. B. *Dalton Trans.* **2006**, 4944.
(31) Sarangi, R.; Aboelella, N.; Fujisawa, K.; Tolman, W. B.; Hedman, B.; Hodgson, K. O.; Solomon, E. I. *J. Am. Chem. Soc.* **2006**, *128*, 8286.
(32) Wurtele, C.; Gaoutchenova, E.; Harms, K.; Holthausen, M. C.; Sundermeyer, J.; Schindler, S. *Angew. Chem., Int. Ed.* **2006**, *45*, 3867.
(33) Lee, D. H.; Hatcher, L. Y. Q.; Vance, M. A.; Sarangi, R.; Milligan, A. E.; Sarjeant, A. A. N.; Incarvito, C. D.; Rheingold, A. L.; Hodgson, K. O.; Hedman, B.; Solomon, E. I.; Karlin, K. D. *Inorg. Chem.* **2007**, *46*, 6056.
(34) Maiti, D.; Fry, H. C.; Woertink, J. S.; Vance, M. A.; Solomon, E. I.; Karlin, K. D. *J. Am. Chem. Soc.* **2007**, *129*, 264.
(35) Lanci, M. P.; Smirnov, V. V.; Cramer, C. J.; Gauchenova, E. V.; Sundermeyer, J.; Roth, J. P. *J. Am. Chem. Soc.* **2007**, *129*, 14697.
(36) Huber, K. P.; Herzberg, G. *Molecular Spectra and Molecular Structure*; Van Nostrand Reinhold: New York, 1979; Vol. 4.
(37) Badger, R. M. *J. Chem. Phys.* **1935**, *3*, 710.
(38) Spencer, D. J. E.; Aboelella, N. W.; Reynolds, A. M.; Holland, P. L.; Tolman, W. B. *J. Am. Chem. Soc.* **2002**, *124*, 2108.
(39) de la Lande, A.; Moliner, V.; Parisel, O. *J. Chem. Phys.* **2007**, *126*.
(40) Cramer, C. J. *Essentials of Computational Chemistry: Theories and Models*, 2nd ed.; John Wiley and Sons: Chichester, 2004.
(41) Reiher, M.; Salomon, O.; Hess, B. A. *Theor. Chem. Acc.* **2001**, *107*, 48.
(42) Bérces, A. *Inorg. Chem.* **1997**, *36*, 4831.
(43) Maddaluno, J.; Geissner-Prettre, C. *Inorg. Chem.* **1991**, *30*, 3439.
(44) Piquemal, J. P.; Pilme, J. *J. Mol. Struct.* **2006**, *764*, 77.
(45) Eisenstein, O.; Getlicherman, H.; Giessner-Prettre, C.; Maddaluno, J. *Inorg. Chem.* **1997**, *36*, 3455.
(46) Liu, X.-Y.; Palacios, A. A.; Novoa, J. J.; Alvarez, S. *Inorg. Chem.* **1998**, *37*, 1202.
(47) Bernardi, F.; Bottoni, A.; Casadio, R.; Fariselli, P.; Rigo, A. *Int. J. Quantum Chem.* **1996**, *58*, 109.
(48) Cramer, C. J.; Smith, B. A.; Tolman, W. B. *J. Am. Chem. Soc.* **1996**, *118*, 11283.
(49) Flock, M.; Pierloot, K. *J. Phys. Chem. A* **1999**, *103*, 95.
(50) Cramer, C. J.; Kinal, A.; Wloch, M.; Piecuch, P.; Gagliardi, L. *J. Phys. Chem. A* **2006**, *110*, 11557.
(51) Cramer, C. J.; Wloch, M.; Piecuch, P.; Puzzarini, C.; Gagliardi, L. *J. Phys. Chem. A* **2006**, *110*, 1991.
(52) Rode, M. F.; Werner, H.-J. *Theor. Chem. Acc.* **2005**, *114*, 309.
(53) Gherman, B. F.; Cramer, C. J. *Coord. Chem. Rev.*, in press; doi: 10.1016/j.ccr.2007.11.018.
(54) Dolg, M.; Wedig, U.; Stoll, H.; Preuss, H. *J. Chem. Phys.* **1987**, *86*, 866.
(55) Hehre, W. J.; Radom, L.; Schleyer, P. v. R.; Pople, J. A. *Ab Initio Molecular Orbital Theory*; Wiley: New York, 1986.
(56) Widmark, P. O.; Malmqvist, P. A.; Roos, B. *Theor. Chim. Acta* **1990**, *77*, 291.
(57) Becke, A. D. *Phys. Rev. A: At., Mol., Opt. Phys.* **1988**, *38*, 3098.
(58) Lee, C.; Yang, W.; Parr, R. G. *Phys. Rev. B: Condens. Matter Mater. Phys.* **1988**, *37*, 785.
(59) Perdew, J. P. In *Electronic Structure of Solids '91*; Ziesche, P., Eschrig, H., Eds.; Akademie Verlag: Berlin, 1991; p 11.
(60) Perdew, J.; Wang, Y. *Phys. Rev. B: Condens. Matter Mater. Phys.* **1992**, *45*, 13244.
(61) Adamo, C.; Barone, V. *J. Chem. Phys.* **1998**, *108*, 664.
(62) Zhao, Y.; Truhlar, D. G. *J. Chem. Phys.* **2006**, *125*, 194101.
(63) Becke, A. D. *J. Chem. Phys.* **1993**, *98*, 5648.
(64) Stephens, P. J.; Devlin, F. J.; Chabalowski, C. F.; Frisch, M. J. *J. Phys. Chem.* **1994**, *98*, 11623.
(65) Zhao, Y.; Truhlar, D. G. *Theor. Chem. Acc.*, in press; doi: 10.1007/s00214-0007-00310-x.
(66) Ziegler, T.; Rauk, A.; Baerends, E. J. *Theor. Chim. Acta* **1977**, *43*, 261.
(67) Noodleman, L.; Norman, J. G. *J. Chem. Phys.* **1979**, *70*, 4903.
(68) Yamaguchi, K.; Jensen, F.; Dorigo, A.; Houk, K. N. *Chem. Phys. Lett.* **1988**, *149*, 537.
(69) Noodleman, L.; Case, D. A. *Adv. Inorg. Chem.* **1992**, *38*, 423.
(70) Lim, M. H.; Worthington, S. E.; Dulles, F. J.; Cramer, C. J. In *Chemical Applications of Density Functional Theory*; Laird, B. B., Ross, R. B., Ziegler, T., Eds.; American Chemical Society: Washington, DC, 1996; Vol. 629, p 402.
(71) Isobe, H.; Takano, Y.; Kitagawa, Y.; Kawakami, T.; Yamanaka, S.; Yamaguchi, K.; Houk, K. N. *Mol. Phys.* **2002**, *100*, 717.
(72) Gräfenstein, J.; Cremer, D. *Mol. Phys.* **2001**, *99*, 981.
(73) Čizek, J. *J. Chem. Phys.* **1966**, *45*, 4256.
(74) Čizek, J. *Adv. Chem. Phys.* **1969**, *14*, 35.
(75) Purvis, G. D.; Bartlett, R. J. *J. Chem. Phys.* **1982**, *76*, 1910.
(76) Scuseria, G. E.; Scheiner, A. C.; Lee, T. J.; Rice, J. E.; Schaefer, H. F. *J. Chem. Phys.* **1987**, *86*, 2881.
(77) Piecuch, P.; Paldus, J. *Int. J. Quantum Chem.* **1989**, *36*, 429.
(78) Kowalski, K.; Piecuch, P. *J. Chem. Phys.* **2000**, *113*, 18.

(79) Piecuch, P.; Kowalski, K. In *Computational Chemistry: Reviews of Current Trends*; Leszczyński, J., Ed.; World Scientific: Singapore, 2000; Vol. 5, p 1.

(80) Piecuch, P.; Kowalski, K.; Pimienta, I. S. O.; McGuire, M. J. *Int. Rev. Phys. Chem.* **2002**, *21*, 527.

(81) Piecuch, P.; Pimienta, I. S. O.; Fan, P.-D.; Kowalski, K. In *Progress in Theoretical Chemistry and Physics*; Maruani, J., Lefebvre, R., Brändas, E., Eds.; Kluwer: Dordrecht, The Netherlands, 2003; Vol. 12, p 119.

(82) Piecuch, P.; Kowalski, K.; Pimienta, I. S. O.; Fan, P.-D.; Lodriguito, M.; McGuire, M. J.; Kucharski, S. A.; Kuś, T.; Musiał, M. *Theor. Chem. Acc.* **2004**, *112*, 349.

(83) Piecuch, P.; Włoch, M.; Lodriguito, M.; Gour, J. R. In *Progress in Theoretical Chemistry and Physics*; Julien, J.-P., Maruani, J., Mayou, D., Wilson, S., Delgado-Barrio, G., Eds.; Springer: Berlin, 2006; Vol. 15, p 45.

(84) Piecuch, P.; Włoch, M.; Varandas, A. J. C. In *Progress in Theoretical Chemistry and Physics*; Lahmar, S., Maruani, J., Wilson, S., Delgado-Barrio, G., Eds.; Springer: Berlin, 2007; Vol. 16, p 65.

(85) Piecuch, P.; Włoch, M. *J. Chem. Phys.* **2005**, *123*, 224105.

(86) Piecuch, P.; Włoch, M.; Gour, J. R.; Kinal, A. *Chem. Phys. Lett.* **2006**, *418*, 467.

(87) Włoch, M.; Lodriguito, M.; Piecuch, P.; Gour, J. R. *Mol. Phys.* **2006**, *104*, 2149.

(88) Włoch, M.; Gour, J. R.; Piecuch, P. *J. Phys. Chem. A* **2007**, *111*, 11359.

(89) Kinal, A.; Piecuch, P. *J. Phys. Chem. A* **2007**, *111*, 734.

(90) Ge, Y.; Gordon, M. S.; Piecuch, P. *J. Chem. Phys.* **2007**, *127*, 174106.

(91) Varandas, A. J. C.; Piecuch, P. *Chem. Phys. Lett.* **2006**, *430*, 448.

(92) Piecuch, P.; Włoch, M.; Varandas, A. J. C. *Theor. Chem. Acc.*, in press; doi: 10.1007/s00214-007-0297-3.

(93) Raghavachari, K.; Trucks, G. W.; Pople, J. A.; Head-Gordon, M. *Chem. Phys. Lett.* **1989**, *157*, 479.

(94) Roos, B. O. In *Ab Initio Methods in Quantum Chemistry*; Lawley, K. P., Ed.; Wiley: New York, 1987; Vol. 2, p 399.

(95) (a) Andersson, K.; Malmqvist, P.-Å.; Roos, B. O.; Sadlej, A. J.; Wolinski, K. *J. Phys. Chem.* **1990**, *94*, 5483. (b) Gagliardi, L. *Theor. Chem. Acc.* **2006**, *116*, 307.

(96) Roos, B. O.; Andersson, K.; Fülscher, M. P.; Serrano-Andrés, L.; Pierloot, K.; Merchán, M.; Molina, V. *J. Mol. Struct.* **1996**, *388*, 257.

(97) Ghigo, G.; Roos, B. O.; Malmqvist, P.-Å. *Chem. Phys. Lett.* **2004**, *396*, 142.

(98) Andersson, K.; Roos, B. O. *Chem. Phys. Lett.* **1992**, *191*, 507.

(99) Merchan, M.; Pou-Amerigo, R.; Roos, B. O. *Chem. Phys. Lett.* **1996**, *252*, 405.

(100) Andersson, K.; Roos, B. O. *Int. J. Quantum Chem.* **1993**, *45*, 591.

(101) Bartmess, J. E. *National Institute of Standards and Technology Webbook*; NIST: Washington, DC; webbook.nist.gov.

(102) Bridge, N. J.; Buckingham, A. D. *Proc. R. Soc. London, Ser. A* **1966**, *295*, 334.

(103) Dewar, M. J. S. *The PMO Theory of Organic Chemistry*; Plenum: New York, 1975.

(104) Bérces, A. *Int. J. Quantum Chem.* **1997**, *65*, 1077.

(105) Alvarez, S.; Palacios, A. A.; Aullon, G. *Coord. Chem. Rev.* **1999**, *186*, 431.

(106) Lewin, J. L.; Heppner, D. E.; Cramer, C. J. *J. Biol. Inorg. Chem.* **2007**, *12*, 1221.

(107) Schipper, P. R. T.; Gritsenko, O. V.; Baerends, E. J. *Theor. Chem. Acc.* **1998**, *99*, 329.